Reactive Fe Anode for Electrolytic Reduction of Solid Metal Oxide in Molten LiCl-Li_2O

[1]Mario Gonzalez, [2]Justin Holland, and [1]Michael Simpson

[1]Department of Materials Science & Engineering, University of Utah, Salt Lake City, Utah

[2]Y-12, Oak Ridge, Tennessee

Abstract

Iron metal was investigated for use as a consumable anode for electrolytic reduction of solid metal oxides in molten LiCl-Li_2O (2 wt%). Tests were performed where the potential of Fe anodes was increased incrementally from 0.1 to 1.0 V (vs Ni/NiO). Oxide formation on the anode started at a potential of 0.4 V and was identified as FeO via X-ray diffraction. In the absence of a pre-formed oxide layer, severe attack of the anode started at a potential of 0.7 V and was accompanied by an increase in Fe concentration in the salt. When an oxide layer was allowed to form on the anode, the Fe concentration did not increase in the salt. O_2 was detected in the headspace gas at an anode potential of 1.0 V only when an oxide layer was present on the anode. The results of this study support the idea that an inexpensive sacrificial anode could be an ideal replacement for expensive Pt that is currently widely used for this process.

1. Introduction

The electrolytic reduction of metal oxides to metal in molten LiCl-Li_2O has been reported by many groups in the open literature [1-9]. In this process, the metal oxide is contained in a stainless-steel basket that is submerged in the molten salt and reduced according to the half-cell reaction shown in equation (1). The anode process relies on the oxidation of O^{2-} ions to form O_2,

as shown in equation (2). In the literature, reports on use of this process have been reported for U, Ti, Nb, Ni, Cr, and Ta [1,2,4,7,9-13].

$$MO_x + 2xe^- \rightarrow M + xO^{2-} \quad (1)$$

$$O^{2-} \rightarrow \frac{1}{2} O_2 + 2e^- \quad (2)$$

The high anodic potential and presence of O^{2-} ions increase the tendency for corrosion at the anode surface, thus making the selection of the anode material very challenging. Traditionally, Pt wires have been used as inert anodes to support the evolution of O_2 during oxide reduction due to the highly inert nature of Pt [14-15]. However, Pt is still susceptible to chemical attack and degradation via the formation of lithium platinate [15-17]. Another problem with Pt is that it is dissolved by metallic lithium [5, 16]. If the cathode reaction produces lithium, it can lead to catastrophic loss of the anode. The high cost of Pt makes its use as a disposable anode an economically unattractive option. Finding an anode material that can withstand the oxidizing conditions in the electrochemical cell is challenging, and the search has focused primarily on materials that are inert and allow for O_2 evolution without significant degradation or corrosion of the anode [18-22].

An alternative approach that has not been extensively studied previously is to make an inexpensive, consumable anode. The use of graphite as a consumable anode material has been studied previously but resulted in contamination of the cathode with carbon via the formation of Li_2CrO_3 [23-25]. Several metals will form metal oxides when anodically polarized in LiCl-Li_2O. A metal that is inexpensive, resists passivation, and does not form a soluble oxide could be an ideal choice for the anode in this process.

For this study, we investigated high-purity iron metal rods as anodes in LiCl-Li_2O. The criteria considered for evaluation of iron metal anodes included the ability to support reduction of the metal oxide, effective utilization of the anode in terms of mass of reduced product per mass of anode consumed, and absence of soluble iron in the salt that could contaminate the reduced product at the cathode.

2. Experimental

2.1 Equipment

All experimental procedures were performed under controlled Ar atmosphere in an Inert Technology glove box with less than 0.1 ppm H_2O. The O_2 concentration in the glove box varied between 8 and 80 ppm throughout experiments. Since O_2 generation can occur during experiments, it is difficult to achieve very low O_2 concentration in the glove box. Thus, the O_2 concentration in the headspace gas was reported for each experiment. A gas sampling system using a peristaltic pump (Masterflex L/S), oxygen sensor (Inert Technologies, EOS-2), and quadrupole mass spectrometer (QMS) (Pfeiffer Vacuum, HiPace 80) was used to detect O_2 and Cl_2 formation throughout experiments. A schematic of the system is shown in Figure 1. The gas sampling system was plumbed into the glovebox using a rubber hose connected to a SS-304 tube which was inserted into the heated zone of the furnace Outside of the glove box, the hose was run through the peristaltic pump, sampling the gas, and flowing it through the oxygen sensor and/or QMS. The oxygen sensor was used to measure the concentration of O_2 in the headspace gas during OR-1 and OR-2. The QMS was set up to analyze the gas qualitatively during OR-2. The QMS scanned atomic masses from 10 – 75 amu and determined a signal for each atomic mass. If the concentration of

any gas changed in the sampled flow, the signal would decrease or increase accordingly for that atomic mass.

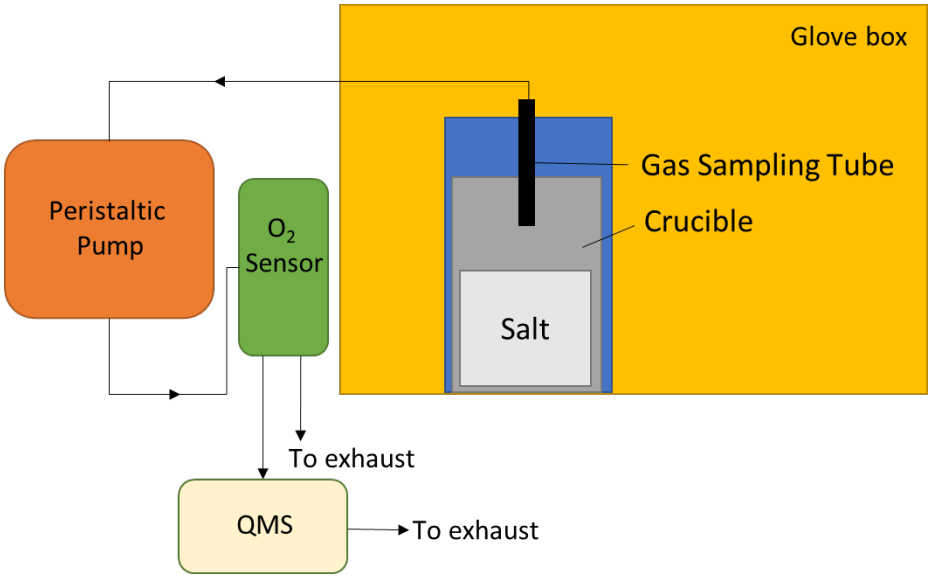

Figure 1. Schematic O_2/Cl_2 detection system using a peristaltic pump, O_2 analyzer, and QMS.

Inside the glove box, the SS tube was inserted into the furnace through a port in a SS-304 heat shield so that it was in the crucible but not in contact with the salt (see Figure 2). A hole was cut through the top of a benchtop muffle furnace (Thermolyne, Thermo Scientific) to interface with the heat shield containing multiple ports allowing for electrode insertion and sampling, also shown in Figure 2. The furnace was used to heat and maintain salt mixtures at 650°C.

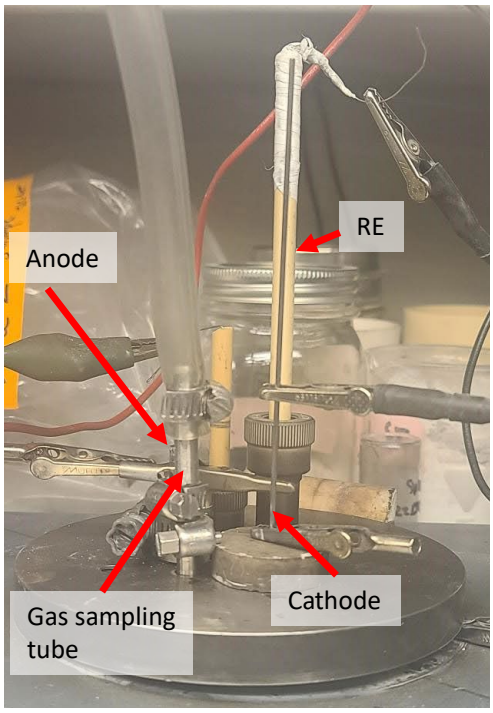

Figure 2. SS heat shield with ports, muffle furnace, and electrode setup used for experiments.

High-density MgO crucibles (Tateho Ozark, 96.5%) were used to contain salt mixtures and were placed inside of a second MgO crucible for secondary containment. Salt temperatures were measured using a Type-K thermocouple (SS-316, OMEGA Engineering). Scanning electron microscopy (SEM) and energy dispersive X-ray spectroscopy (EDS) analyses were performed using a Hitachi TM3030Plus Tabletop SEM with EDS capabilities. ICP-MS analysis was performed using an Agilent ICP-MS 7900 quadrupole mass spectrometry system. XRD analysis was performed using a Bruker D2 Phaser XRD. Elemental oxygen analysis was performed using a TCH600-Nitrogen/Oxygen/Hydrogen Determinator. Titrations were performed using a Titroline® 7000 auto-titrator.

2.2 Materials and Reagents

Molten salt mixtures were prepared using anhydrous LiCl (anhydrous, Sigma-Aldrich 99%+) and Li_2O (Alfa Aesar, 99.5%). Reference electrodes were made using MgO (Tateho Ozark, 96.5%) tubes filled with NiO (99.99%, Alfa Aesar) with a Ni wire (99.98%, Thermo Scientific) inserted. Fe rods (Alfa Aesar, 99.95%) were used as anodes. UO_2 powder (New Brunswick Laboratory), a cylindrical UO_2 pellet (25 g, 15-mm diameter, 17-mm height, INL), and a W rod (Alfa Aesar, 99.5%) were used as cathodes.

2.3 Salt Preparation

LiCl used in these experiments was pre-dried following the established procedure for removing residual moisture from LiCl-based melts [26, 27]. First, LiCl was heated from ambient temperature to 120°C at a rate of 5^oCmin^{-1}. The LiCl was then held at 120, 270, 470, and 200°C for time intervals described in the previously published procedure before allowing it to cool to ambient temperature [26, 27]. LiCl-Li_2O mixtures were made by adding Li_2O to pre-dried LiCl at room temperature and heating to 650°C at a rate of 15^oCmin^{-1}. Molten LiCl-Li_2O mixtures were treated with Li metal following the reported procedure for removing LiOH contamination via metallothermic reduction of LiOH to Li_2O [27]. The Li_2O concentration of prepared salt mixtures was determined via titration.

2.3 Electrowinning and Oxide Reduction Experiments

Three electrochemical experiments were performed using a three-electrode (anode, cathode, reference electrode) configuration. In all cases, the reference electrode (RE) was Ni/NiO enclosed in a MgO tube with ½" long porous plug. The anode signal was controlled, monitored,

and recorded using an Autolab PGSTAT302N potentiostat. The cathode signal was monitored and recorded using an Agilent 34450A multimeter. The RE was inserted in the salt before melting and heated alongside the salt. The cathode was immersed in the salt once the salt was molten. A vertical translator made from a motorized Velmex BiSlide was used to control anode immersion depth. With the RE and cathode in the molten salt, the anode was lowered incrementally (0.25-mm steps) until the potentiostat indicated that the resistance between the cathode and anode was not infinite. The anode was then lowered into the salt to the desired immersion depth. This method resulted in an immersion depth within ~0.25mm precision. Current densities were reported based on the initial anode surface area in contact with the electrolyte at the start of the test.

An electrowinning (EW) experiment (EW-1) was run in LiCl containing 2.0 wt% Li_2O. The anode was a 7.6-mm diameter Fe rod, and the cathode was a 3.2-mm diameter W rod. This experiment was run for 18 minutes in constant potential mode after setting the anode potential at 1.0 V versus Ni/NiO.

Oxide reduction (OR) experiment OR-1 was run in LiCl initially containing 2.4 wt% Li_2O. The cathode was UO_2 powder (106 – 1000 μm) in a SS (SS-304) basket assembly lined with 37-μm SS mesh (304 SS). The cathode basket assembly (see Figure 3a), originally reported by Burak et al. [28], is designed to avoid polarization of the SS basket and promote UO_2 reduction. This experiment used a single 7.6-mm diameter Fe rod as the anode with an immersion depth of 3.05 cm and initial contact area of 7.74 cm^2. This experiment was run as a series of approximately 10-min segments during which the anode potential was increased incrementally in 0.1 V steps from 0.2 to 1.0 V. The anode was inspected visually between each anode potential hold stage and then placed back into the salt for the next step. Each segment of the experiment used the same salt and Fe anode.

Oxide reduction experiment OR-2 was run in LiCl initially containing 2.1 wt% Li_2O. The cathode was a UO_2 pellet, wrapped tightly in stainless-steel wire (see Figure 3b). The UO_2 pellet was immersed in the salt entirely. This experiment used 3.1-mm diameter Fe rods as anodes with an immersion depth of 1.5 cm, resulting in an initial contact area of 1.53 cm^2. OR-2 was run as a series of 10 segments where the anode basket potential was increased incrementally in 0.1 V steps from 0.1 to 1.0 V. During this experiment, the Fe anode was replaced before each new potential step.

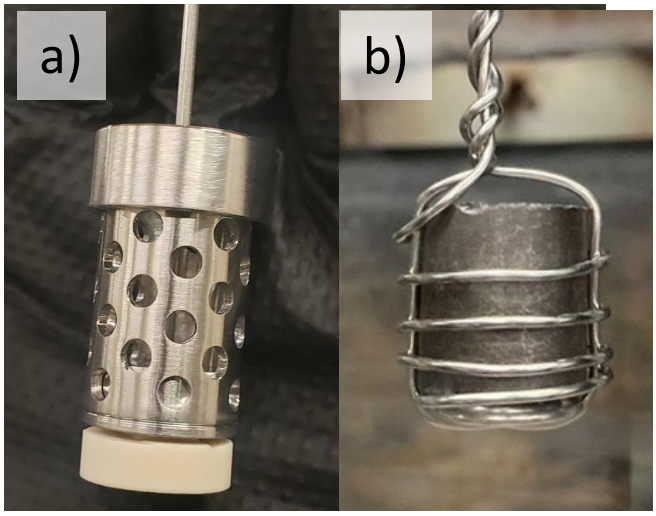

Figure 3. (a) SS basket assembly filled it UO_2 powder used as the cathode in OR-1 and the (b) UO_2 pellet used as the cathode in OR-2.

2.4 Analysis and Characterization

Bulk salt samples were taken using a stainless steel (304 SS) threaded rod. The threaded rod was inserted into the salt and removed quickly, allowing the salt to adhere and solidify. Titrations of salt samples were performed in triplicate using an SI Analytics Titroline 7000 autotitrator and reported as averages. Inductively coupled plasma mass spectroscopy (ICP-MS) analysis was performed on samples in triplicate and results are reported as averages.

When sufficient buildup was formed on the anode, the buildup was removed from the anode with pliers and rinsed with DI water to move residual salt. The material was then air-dried before XRD analysis.

In experiments where crucibles were broken to recover settled material after experiments, salt was rinsed off the settled material with DI water, and the material was recovered via vacuum filtration. The recovered material was air-dried before XRD analysis.

3. Results

3.1 Electrowinning in LiCl-Li_2O with a W Cathode

An electrowinning experiment (EW-1) was run using an Fe anode and W cathode to determine potential response to a constant current when excluding UO_2 from the cathode. Reduction at the cathode could only involve lithium compounds in the salt such as LiCl, Li_2O, and LiOH. This should allow distinction between cathode potentials indicative of UO_2 and those indicative of Li^+ reduction (equation (3)) or OH^- reduction (equation (4)).

$$Li^+ + e^- \rightarrow Li \qquad (3)$$

$$OH^- + e- \rightarrow O^{2-} + \tfrac{1}{2}H_2 \qquad (4)$$

The current and cathode potential recorded during test EW-1 are shown in Figure 4. The potential at the W cathode ranged from -1.90 to -1.78 V vs Ni/NiO. There was a step change in the current signal approximately 2.5 minutes into the experiment where the current was halved for one minute. The step change can also be seen in the cathode potential. The cause of the drop in current is unknown.

Following OR-1, a soft metallic deposit was collected from the W cathode. This deposit was added to a beaker of DI water where it off-gassed vigorously before reacting completely.

178 Titration of salt samples before and after the test indicated that Li_2O concentration in the salt
179 decreased from 2.00 to 1.23 wt%. The decrease in Li_2O concentration in the salt could have only
180 occurred via a net removal of O^{2-} from the system via the formation of O_2 or iron oxide. This
181 eliminates LiCl electrolysis as the cathode reaction, since LiCl electrolysis would not have
182 changed the O^{2-} concentration in the salt. In titration, LiOH and Li_2O are indistinguishable because
183 Li_2O reacts with water to form LiOH. Thus, both LiOH and Li_2O yield OH^- in the titration solution.
184 If reduction of OH^- (equation (4)) to O^{2-} was occurring at the cathode, the results of titration would
185 have shown no change in the O^{2-} concentration in the salt. This eliminates OH^- reduction as the
186 cathode reaction. Thus, it was confirmed that Li metal formed from reduction of Li^+ ions at the
187 cathode between -1.90 and -1.78 V versus our Ni/NiO RE. This is consistent with the findings of
188 Herrmann et al. who report that Li^+ reduction occurs at potentials more negative than -1.78 V vs
189 Ni/NiO [29].
190

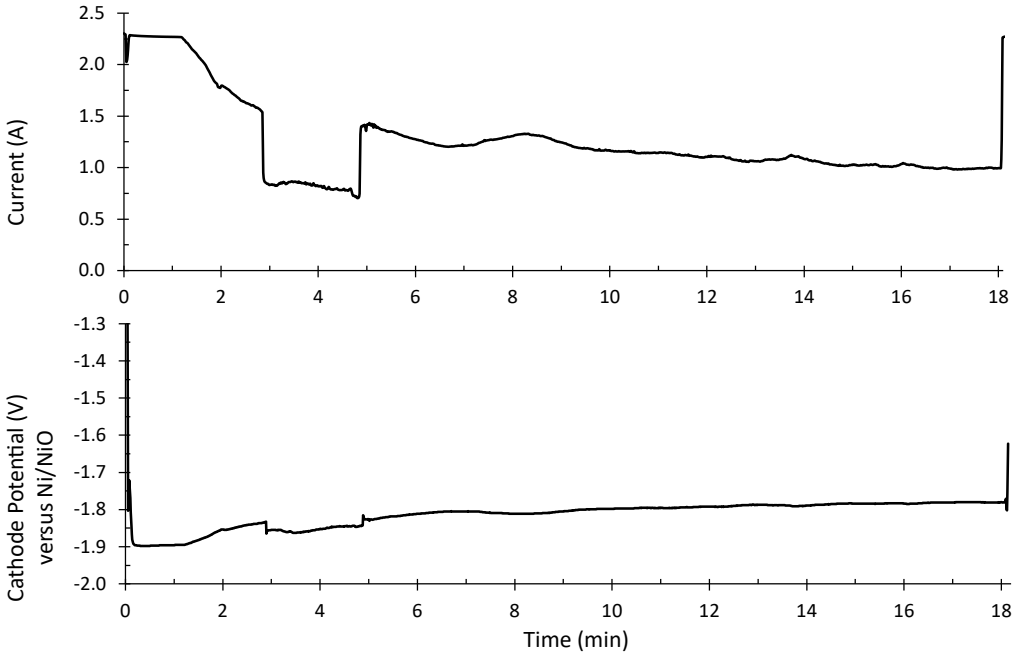

Figure 4. Electrode response signals during electrowinning test EW-1 in LiCl-2wt%Li_2O at 650ºC with Fe anode, W cathode, and Ni/NiO RE.

Previously, LiOH contamination was reported as the leading cause of reductive current beginning at -0.75 V vs Ni/NiO and preceding Li_2O reduction in LiCl-Li_2O at 650ºC [27] and should be included as a possible cathode reaction. The results of this test were used in conjunction with those of Sakamura et al. who found that UO_2 reduction begins + 0.15 V vs Li^+/Li in LiCl at 650ºC [1] and Herrmann et al. who found that electrolytic UO_2 reduction begins at -1.57 V versus Ni/NiO in LiCl-Li_2O at 650ºC [29] to build a reduction a profile (see Figure 5). This profile allows for distinction between the three main cathode processes that can occur during OR experiments.

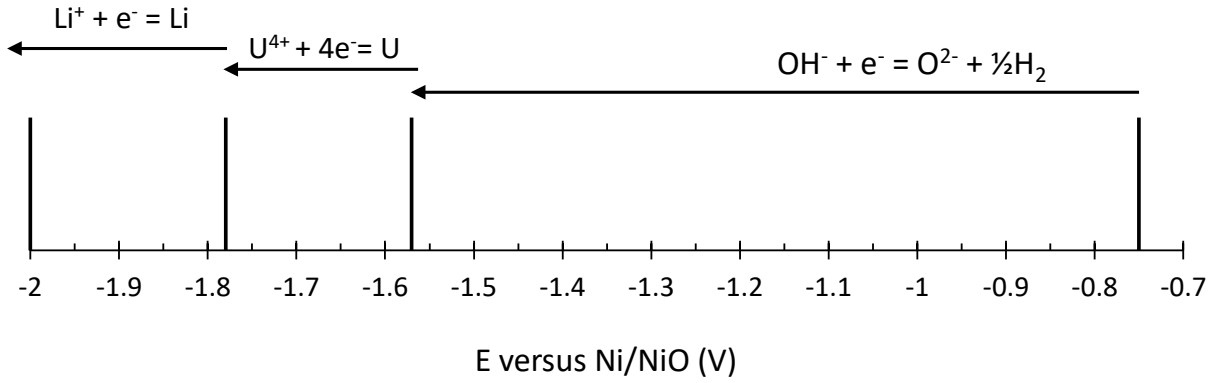

Figure 5. Reduction potential profile for the UO_2-Li_2O-LiOH-LiCl system at 650°C.

Figure 6 shows a photograph of the Fe anode after experiment EW-1 and the XRD pattern for the recovered anode product. The results of XRD indicate that only metallic Fe was present. This was initially unexpected because iron oxide was anticipated as a product of the anode reaction. The measured decrease in Li_2O could only result in formation of iron oxide at the anode or formation of O_2 gas.

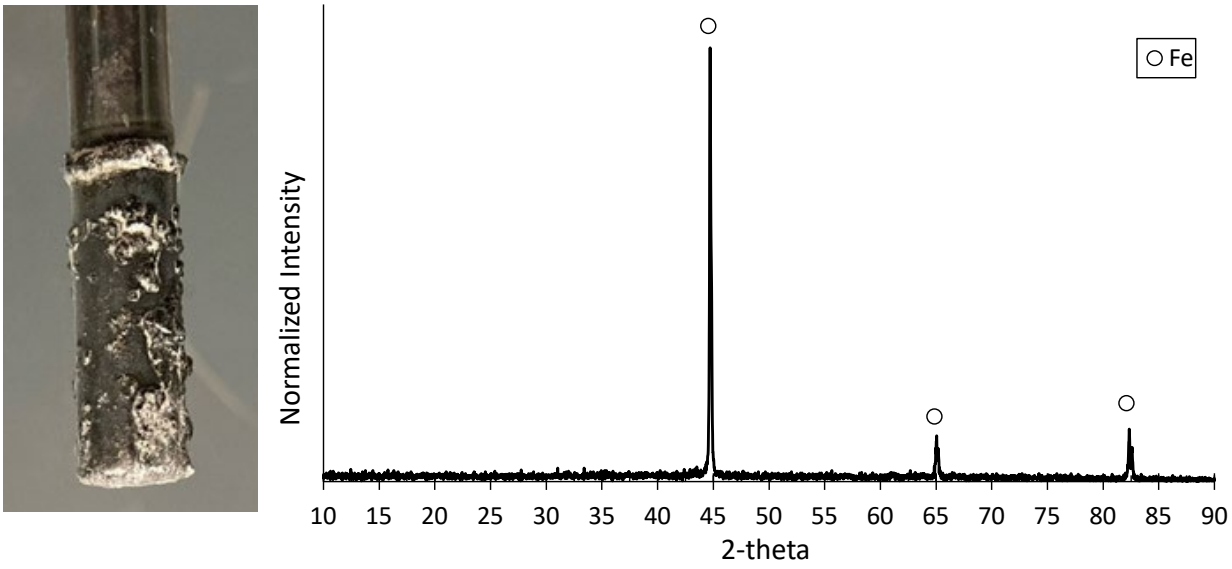

Figure 6. Photograph of Fe anode and XRD pattern for material recovered from the Fe anode after experiment EW-1.

214

215 *3.2 Oxide Reduction using UO_2 Cathode*

216 Two OR experiments (OR-1 and OR-2) were performed with iron anodes in LiCl-Li_2O
217 with UO_2 cathodes. A summary of conditions and results for experiments OR-1 and OR-2 is shown
218 in Table I.

219

220 **Table I.** Summary of conditions and results for experiments OR-1 and OR-2.

Test	Anode	Cathode	Anode Potential (V)	DT (min)	Cum. Charge I	Initial O_2 (ppm)	Final O_2 (ppm)
OR-1	One Fe anode throughout experiment	UO_2 Powder in SS basket	0.2	12.3	87	8.9	8.9
			0.3	11.7	96	8.8	8.8
			0.4	11.9	157	8.9	8.9
			0.5	10.9	190	8.8	8.8
			0.6	10.8	263	8.8	9.2
			0.7	11.1	318	8.9	9.1
			0.8	12.5	324	8.8	9.1
			0.9	10.9	370	8.9	9.2
			1.0	10.5	693	8.9	999.7
OR-2	Fe anodes replaced between each potential step.	UO_2 pellet wrapped in SS-wire	0.1	30	38	73.2	67.5
			0.2	30	42	55.4	53.5
			0.3	30	61	54.5	54.9
			0.4	30	166	55.5	57.2
			0.5	30	155	57.6	51.3
			0.6	30	337	48.5	45.1
			0.7	30	1638	48.8	42.8
			0.8	15	669	39.8	41.4
			0.9	15	607	38.1	40.9
			1.0	15	971	35.9	37.0

221
222
223 In each OR test, fixed anode potential segments were run successively in a single batch of
224 salt. Experiment OR-1 used a single Fe anode and a UO_2 powder cathode. It was run as a series of
225 segments with a duration (DT) of approximately 10 minutes, resulting in a cumulative time of
226 102.7 min with 2498 C of total charge passed. In experiment OR-2, the Fe anode was replaced

after each constant potential segment, and a UO_2 pellet was used as the cathode. Electrical signals measured at anodes throughout experiments OR-1 and OR-2 are shown in Figures 7 and 8, respectively.

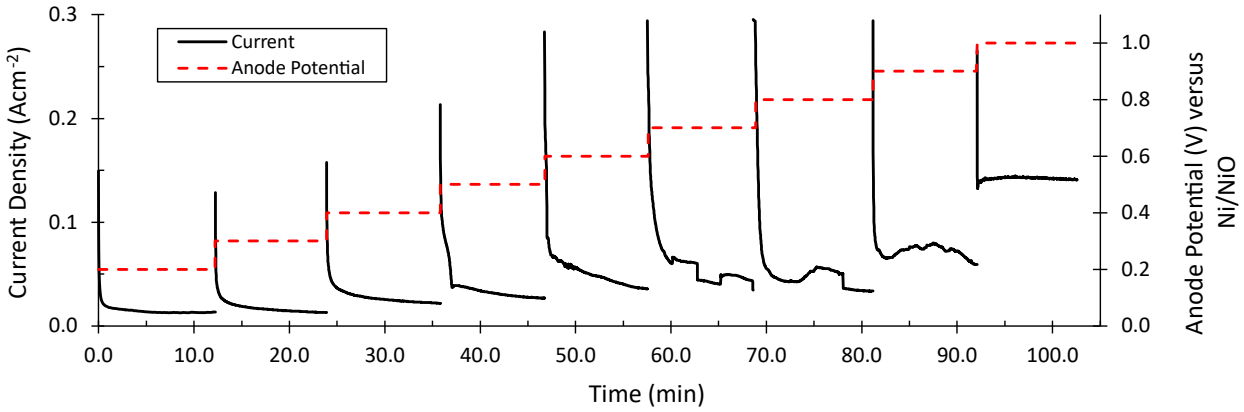

Figure 7. Anode current density and potential throughout OR-1.

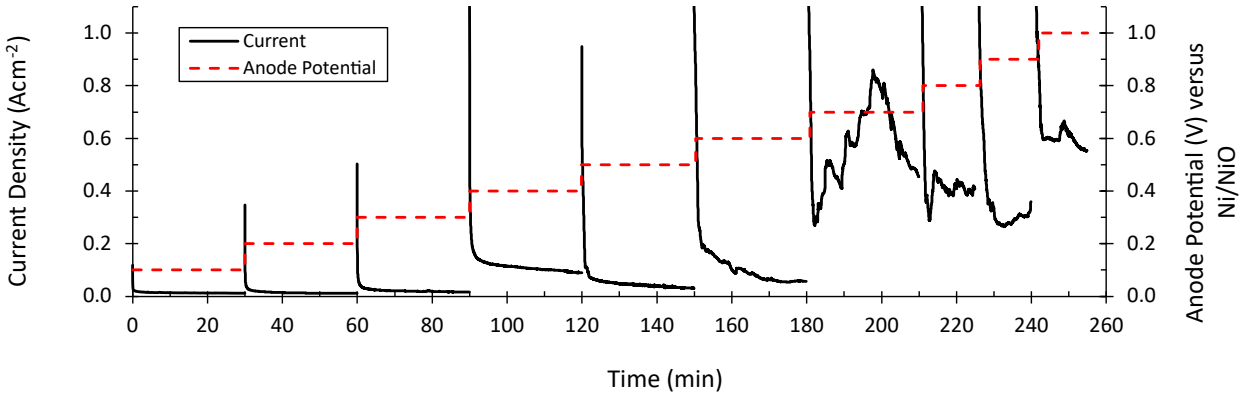

Figure 8. Anode current density and potential throughout OR-2.

Figure 9 shows the Li_2O concentration throughout tests OR-1 and OR-2 measured via titration. The Li_2O concentration was constant within the experimental error for both tests. The constant concentrations indicate that there was a balance of removal and replacement of O^{2-} ions

in the salt during both runs. That eliminates electrowinning of Li_2O from the reaction mechanism. The UO_2 must have provided an influx of O^{2-} ions into the salt, which balances their consumption at the anode. In test EW-1 in which there was no UO_2 in the cathode, the Li_2O concentration decreased from 2.0 to 1.2 wt%, consistent with Li_2O electrowinning. Thus, we successfully showed that the Fe anode supports Li_2O electrowinning in the absence of a UO_2 cathode and oxide reduction of UO_2 when using a UO_2 cathode. The cumulative charge of 693 and 971 C for OR-1 and OR-2, respectively, would cause the Li_2O concentration to drop to the levels shown by the dashed lines in Figure 9 if Li_2O electrowinning was the dominant reaction in OR-1 and OR-2.

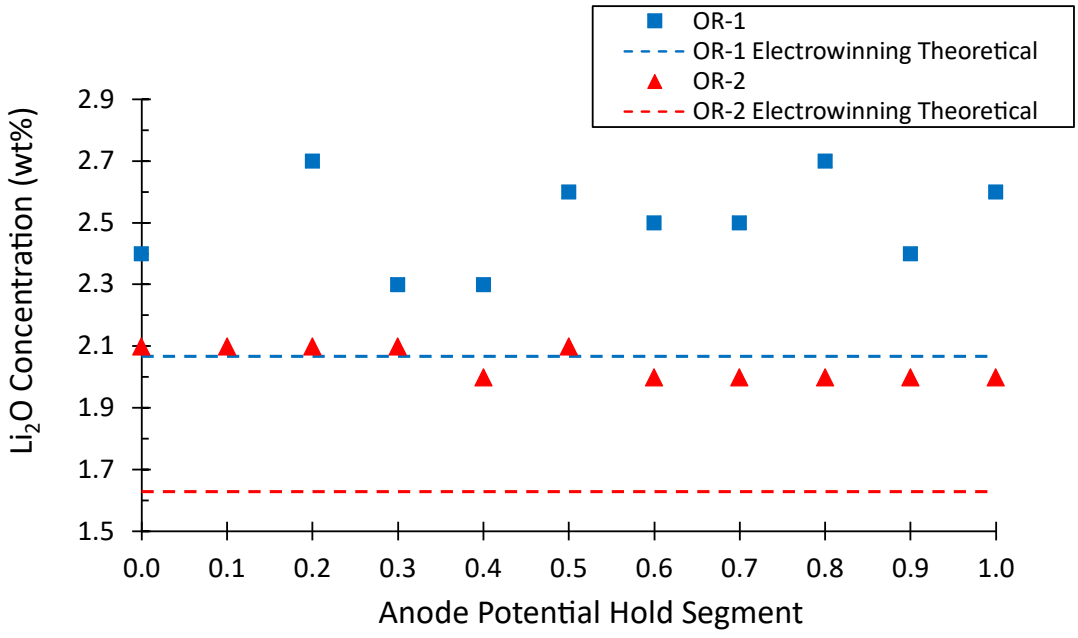

Figure 9. Li_2O concentration in salt samples taken during experiments OR-1 and OR-2, measured via titration.

Photographs of the single Fe anode used throughout experiment OR-1 are shown in Figure 10. In all cases except the 0.5 V step, the Fe anode was removed promptly after each potential

increase step, and a photograph was taken. No visible iron oxide formation was noted during the 0.2 and 0.3 V steps. Iron oxide buildup on the anode surface was observed starting at 0.4 V. No material was removed from the anode between steps. After the 0.5 V step, the Fe anode was left immersed in the salt for an hour with no applied potential, and the anode rod looked clean after removal from the salt. Starting at an anode potential of 0.6 V, a uniform oxide layer formed in the region that was immersed in the salt with a larger diameter buildup right above the salt layer. There was no visible constriction of the Fe anode at any point along its length during experiment OR-1. As reported in Table I, the O_2 concentration in the headspace remained low and constant until the anode potential was raised to 1.0 V. At this point, the O_2 concentration rose to 999.7 ppm in the first five minutes of the test, which is the maximum reading for the O_2 sensor. This indicates that O_2 can form on the surface of the Fe anode at 1.0 V (vs Ni/NiO) given sufficient passivation with what appears to be an oxide layer.

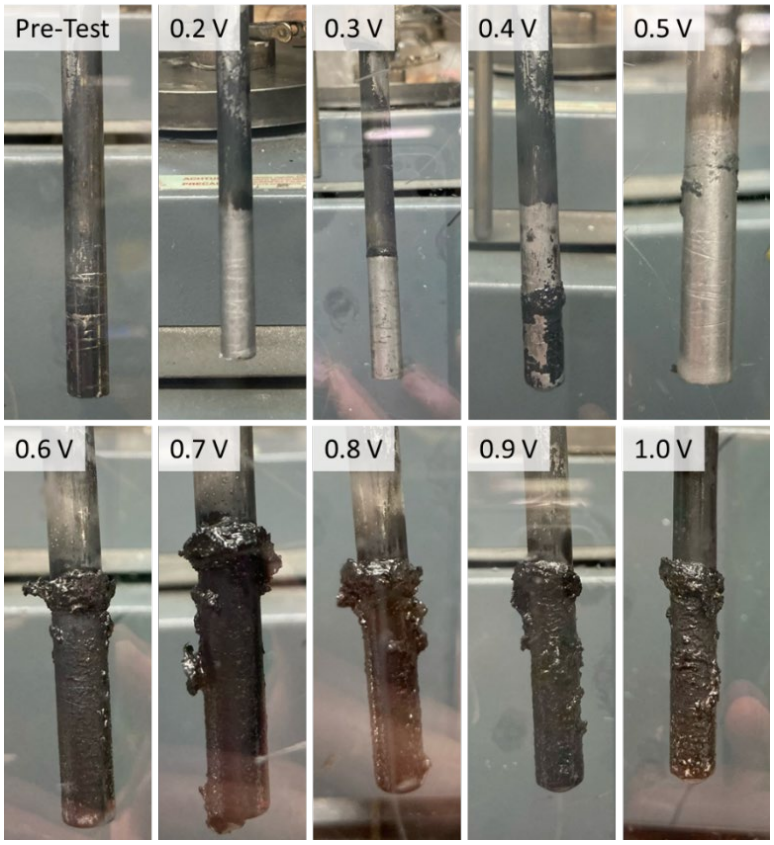

Figure 10. Fe anode before and after each potential step during experiment OR-1

The material that built up on the surface of the anode in experiment OR-1 was analyzed via XRD, and the results are shown in Figure 11. The most prominent peaks in the XRD pattern matched FeO. The results of elemental oxygen analysis of a sample of the material that could be removed from the anode indicate that the oxide contained an O concentration of 4.8 wt%. This O concentration is too low for FeO (22.3 wt% O) or any known form of Fe_xO_y. The high background in the XRD pattern made it difficult to identify other peaks. Another consideration is that the sample removed from the anode could have contained a mixture of FeO and Fe.

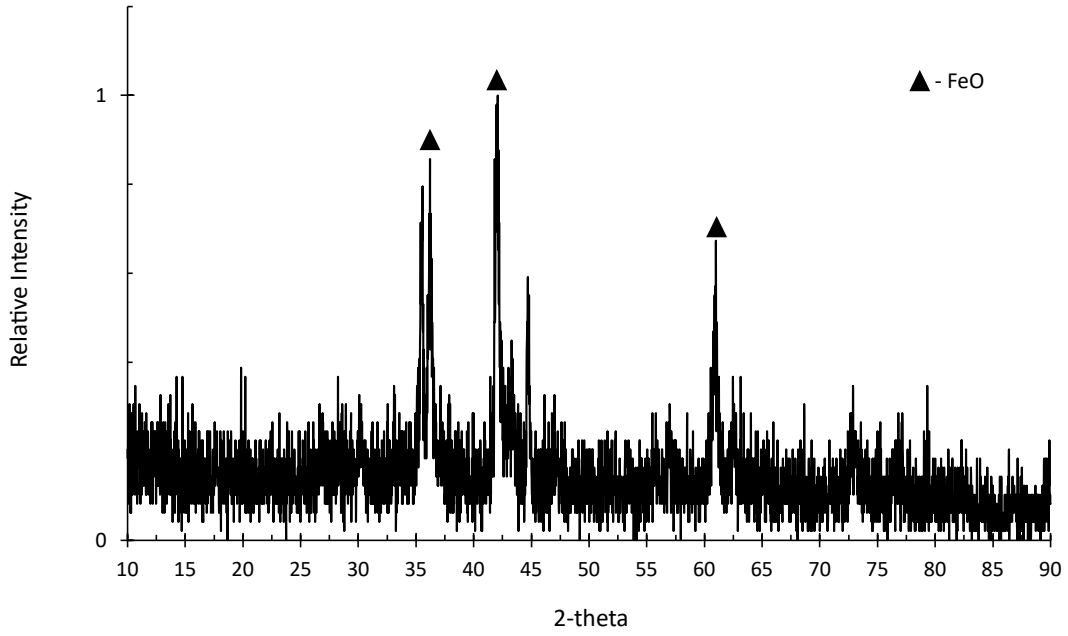

Figure 11. XRD pattern for material recovered from the Fe anode after experiment OR-1.

In experiment OR-2, Fe anodes were replaced before each new potential step to observe how the oxide layers formed without cumulative buildup over the full potential range. Photographs of anodes used in OR-2 are shown in Figure 12. Buildup appeared on the surface of anodes starting at an anode potential of 0.4 V without any visible anode constriction. Severe anode constriction was observed starting at an anode potential of 0.7 V which required shortening of the remaining test segments. The observed constriction for anodes polarized at 0.7 V and higher shows the importance of building up a passivation layer at lower potentials. No anode constriction was observed at any potential up to and including 1.0 V in test OR-1. Such constriction could be explained by the formation of soluble iron chloride via the reactions shown in equations (5) and (6). These reactions are undesirable since they consume the anode without achieving productive oxide reduction.

$$Fe + 2Cl^- \rightarrow FeCl_2 + 2e^- \quad (5)$$

$$Fe + 3Cl^- \rightarrow FeCl_3 + 3e^- \quad (6)$$

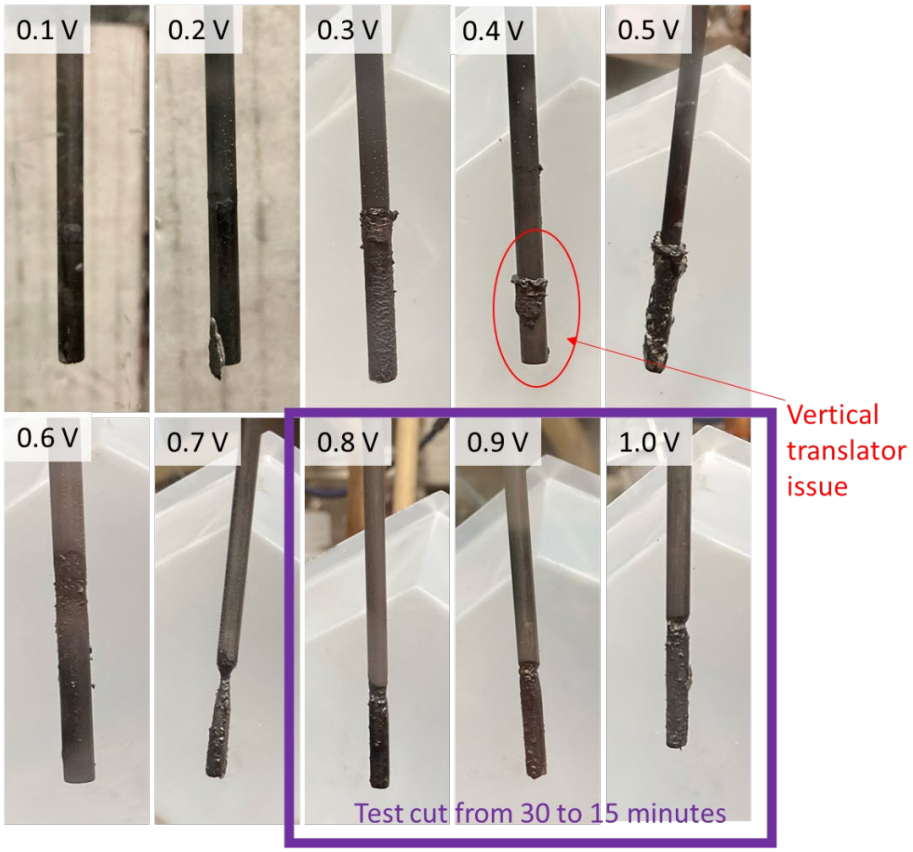

Figure 12. Fe anode after each potential step during DER-2

In experiment OR-2, there was no discernable increase in concentration of O_2 in the sampled headspace gas. Thus, it was concluded that O_2 generation did not occur during the experiment. Inspection of the salt after OR-2 revealed a large amount of settled material at the bottom of the crucible (see Figure 13). XRD analysis was performed on the accumulated product

306 that settled at the bottom of the crucible throughout test OR-2. The results of the XRD analysis are
307 also shown in Figure 13. The settled material, recovered after OR-2, matched Fe.
308
309

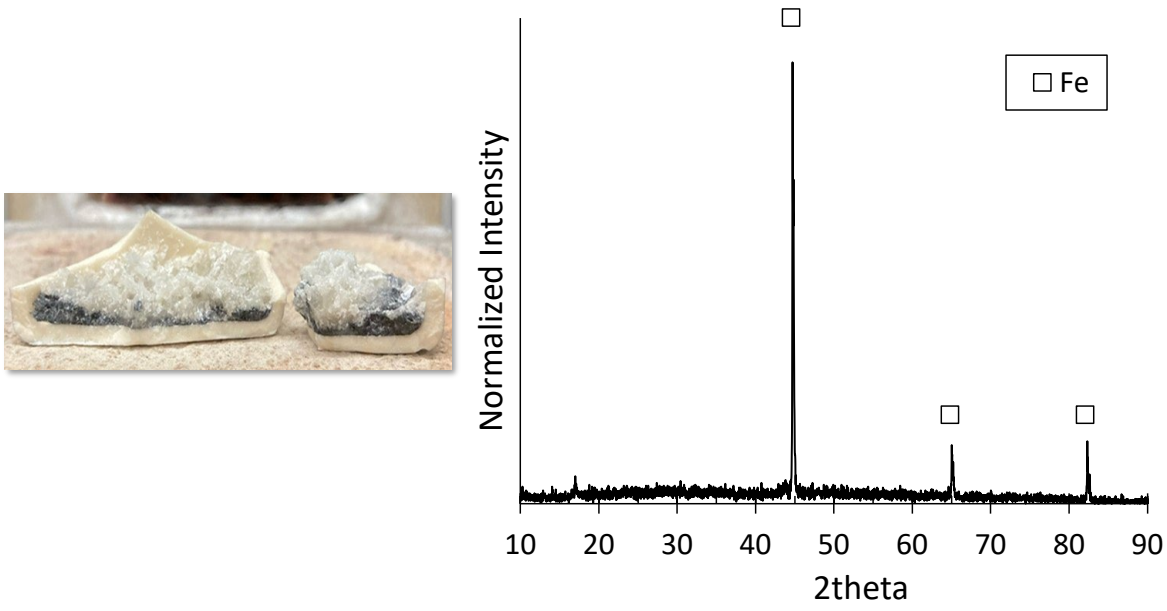

310
311 **Figure 13.** Photograph of broken crucible with dark settled material OR-2 and matched XRD for
312 the recovered settled material.
313
314 ICP-MS analysis was performed on salt samples taken throughout experiments to
315 determine whether soluble Fe was entering the salt. The results of ICP-MS analysis are shown in
316 Figure 14. In experiment OR-1, where a SS cathode basket was used, the concentration of Fe in
317 the salt did not change appreciably throughout the test, and the highest concentration of Fe in the
318 salt was 0.05 wt%. This provides more evidence that equations (5) and (6) are prevented by proper
319 passivation of the anode at lower potentials. In experiment OR-2, the Fe concentration increased
320 10x during the 0.7 V step and remained elevated for the remainder of the test, reaching a maximum
321 of 0.52 wt%. The increase in Fe concentration in the salt in OR-2 is consistent with the reactions

shown in equations (5) and (6). At the cathode, Fe metal could have been deposited and fallen off to the bottom of the crucible to yield the material collected and shown in Figure 13. Also in support of equations (5) or (6) is the lack of a signal for Cl_2 in qualitative QMS analysis of the headspace gas throughout OR-2.

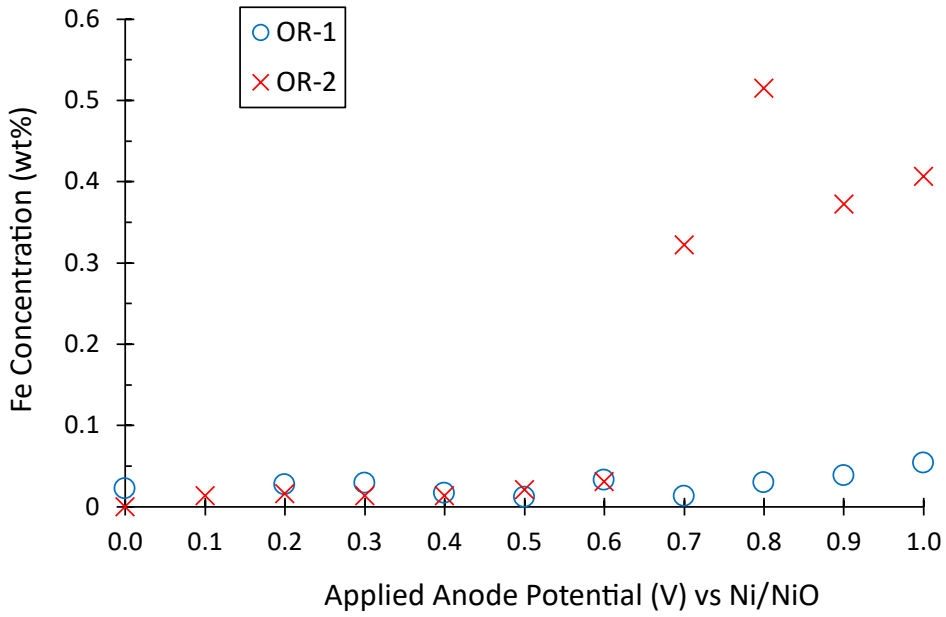

Figure 14. Results of ICP-MS analysis of bulk salt samples taken throughout OR-1 and OR-2.

4. Discussion

4.1 Fe Anode Oxidation

The results of OR experiments indicate that the formation of oxides at the anode precedes O_2 evolution. During test OR-1, O_2 was not detected in the headspace gas until the anode potential reached 1.0 V. In test OR-2, O_2 was not detected for any anode potential. In both cases oxide material formed on the iron anode(s). Further evidence of this can be provided using thermodynamic calculations. Equations (7) and (8) show reactions and free energies of reaction resulting in the formation of FeO and O_2 at 650°C , respectively.

$Fe + Li_2O = FeO + 2Li$ $\Delta G_{rxn}^{o} = 272$ kJ/mol (7)

$Li_2O = \frac{1}{2}O_2 + 2Li$ $\Delta G_{rxn}^{o} = 476$ kJ/mol (8)

The relationship shown in equation (9) describes the relationship between Gibb's free energy and reduction potential where ΔG is the Gibb's free energy in J, E is the standard reduction potential in V, n is the number of electrons transferred, and F is Faraday's constant in C/mol e^-.

$$E = -\frac{\Delta G}{nF} \quad (9)$$

Using equation (9), the standard state free energy of equations (7) and (7) can be used to estimate the potential difference between FeO and O_2 formation from the reduction of Li_2O. The resulting standard reduction potentials are -1.41 V for FeO and -2.47 V for O_2 generation, resulting in a potential difference of 1.07 V. Since the potential needed for equation (7) is less negative than that of equation (8), these calculations also indicate that the formation of FeO precedes that of O_2.

Results of XRD analysis of the anode product after OR-1 confirm the presence of FeO. While there is evidence of additional peaks that could belong to other forms of iron, such as Fe_2O_3 (2θ: 35.6, 43.4, 60.9, 68.6, 72.8, and 79.5°), the only clear additional peak is the peak at 2θ 35.6°. The peak at 2θ 60.9 is shared with FeO, and the remaining peaks are much too close to background to identify confidently. The fluorescence of Fe in response to incident Cu X-rays generated by the XRD leads to a large background that makes the identification of distinct iron oxides phases difficult [30, 31]. If the anode oxide is a mixed oxide, XRD analysis is insufficient for identification of iron oxide phases. X-Ray absorption spectroscopy (XAS) has been reported as a more suitable method for iron oxide phase identification in crystalline solids [31, 32] and could allow for better characterization of the anode oxides.

4.2 Soluble Fe Formation and Anode Depletion

In the absence of a passivating oxide layer, extensive anode depletion begins at around 0.7 V vs Ni/NiO (see Figure 12) and is accompanied by soluble Fe entering the salt (see Figure 14). The maximum concentration of Fe measured in the salt was 10x higher in OR-2 (0.5 wt% Fe), where a passivating oxide layer was not allowed to form on Fe anodes, than in OR-1 (0.05 wt% Fe). This is consistent with the depletion of the Fe anode during the 0.7 V step of OR-2 (see Figure 12). The lack of an increase in Fe concentration in the salt during OR-1 indicates that the passivation of Fe anodes with oxides minimizes the amount of soluble Fe that enters the salt and protects the anode from further depletion.

While the concentration of Fe in the salt did not increase during OR-1, a metallic-appearing deposit did form on the cathode basket as shown in Figure 15. The accompanying XRD of this material verified that it contained Fe. UO_2 was also detected identified by the XRD, which is expected given that the basket was initially loaded with UO_2. Thus, it appears that Fe electrorefining also occurred, probably to a lesser extent in OR-1. Thus, this is a competitive reaction for the Fe anodes that must be monitored and mitigated.

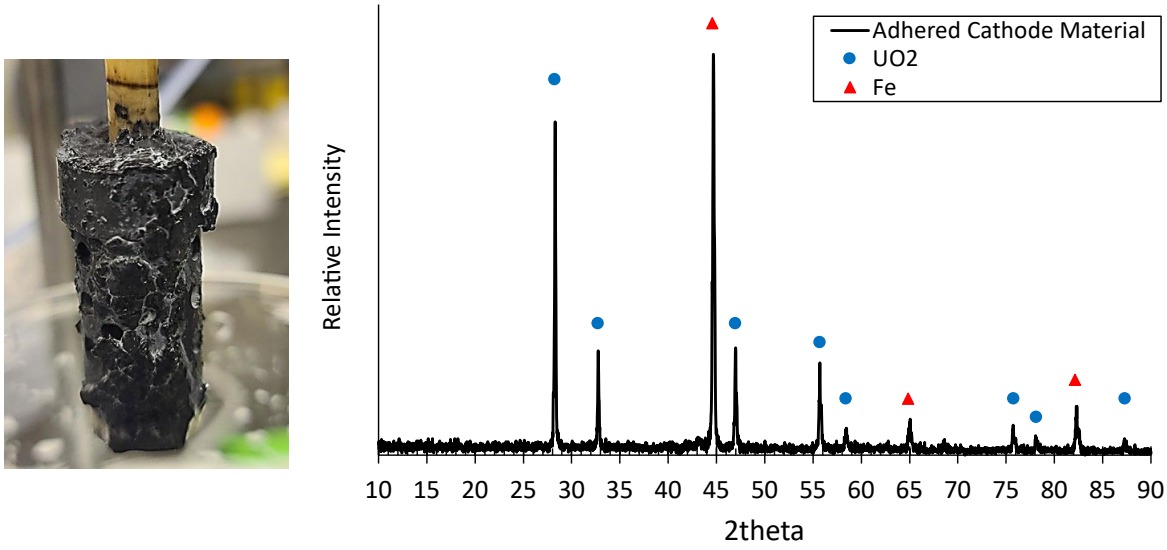

Figure 15. (a) Photo of cathode basket for OR-1 with adhered material, (b) XRD of adhered material.

Equations (10) and (11) show the possible mechanisms and free energies of reactions resulting in $FeCl_x$ formation via reaction of LiCl and O_2 with FeO and Fe at 650°C, respectively. The free energies of reaction indicate that formation of $FeCl_x$ is favorable on a fresh Fe surface and not one that has been passivated with FeO. This would explain why there was an increase in Fe concentration in the salt during OR-2 but not OR-1.

$$FeO + 3LiCl + \tfrac{1}{4}O_2 = FeCl_3 + \tfrac{3}{2}Li_2O \qquad \Delta G_{rxn}^{o} = 1034\ kJ/mol \qquad (10)$$

$$Fe + LiCl + \tfrac{1}{2}O_2 = \tfrac{1}{2}FeCl_2 + \tfrac{1}{2}Li_2O + \tfrac{1}{2}FeO \qquad \Delta G_{rxn}^{o} = -238\ kJ/mol \qquad (11)$$

Furthermore, the reaction shown in equation (11) results in the formation of FeO, which was identified in the settled particulate at the bottom of the crucible after test EW-1 (refer to Figure 11).

5. Conclusions

Sacrificial iron metal anodes were shown to be promising for use in oxide reduction of solid metal oxides such as UO_2 in molten LiCl-Li_2O salt. The formation of a passivating oxide layer on Fe anodes starting at an anode potential of 0.3 to 0.4 V relative to Ni/NiO reference electrode precedes O_2 generation which starts at an anode potential of 1.0 V. When using a UO_2 cathode, oxide reduction of the metal occurs rather than electrowinning of Li_2O. Soluble iron chloride formation appears to initiate at 0.7 V in the absence of an iron oxide passivating later. Cl_2 does not form on iron anodes at least up to a potential of 1.0 V. Salt soluble Fe is electrochemically active and can result in Fe anode electrorefining, which is unproductive and should be avoided.

References:

1. Sakamura, Yoshiharu, Masaki Kurata, and Tadashi Inoue. "Electrochemical reduction of UO_2 in molten $CaCl_2$ or LiCl." Journal of the Electrochemical Society 153.3 (2006): D31.

2. Herrmann, S. D., and S. X. L“. "Separation and recovery of uranium metal from spent light water reactor fuel via electrolytic reduction and electrorefining”." *Nuclear Technology* 171.3 (2010): 247-265.

3. Lee H, Park G-I, Kang K-H, et al. Pyroprocessing technology developments at KAERI. *Nucl Eng Technol*. 2011;43(4):317-328. doi:10.5516/NET.2011.43.4.317

4. Seo C.S., Park S.B., Park B.H., Jung K.J., Park S.W., Kim S.H. Electrochemical study on the reduction mechanism of uranium oxide in a LiCl-Li_2O molten salt. Journal Nuclear Science and Technology. 45, no. 5 (2006) 587-595.

5. Herrmann S, Li S, Simpson M. Electrolytic reduction of spent light water reactor fuel bench-scale experiment results. *J Nucl Sci Technol*. 2007;44(3):361-367. Doi:10.1080/18811248.2007.9711295

6. Hur JM, Jeong SM, Lee H. Underpotential deposition of Li in a molten LiCl-Li_2O electrolyte for the electrochemical reduction of U from uranium oxides. *Electrochem commun*. 2010;12(5):706-709. doi:10.1016/j.elecom.2010.03.012

7. Choi EY, Jeong SM. Electrochemical processing of spent nuclear fuels: An overview of oxide reduction in pyroprocessing technology. *Prog Nat Sci Mater Int*. 2015;25(6):572-582. doi:10.1016/j.pnsc.2015.11.001

8. Yoo JH, Seo CS, Kim EH, Lee HS. A conceptual study of pyroprocessing for recovering actinides from spent oxide fuels. Nucl Eng Technol. 2008;40(7):581-592. doi:10.5516/NET.2008.40.7.581

9. Park S.B., Seo C.S., Kang D.S., Kwon S.G., Park S.W. Study of the Electrolytic Reduction of Uranium Oxide in LiCl-Li_2O Molten Salts with an Integrated Cathode Assembly. J. Korean Radioactive Waste Society, vol. 3(2), 105-112, 2005.

10. Chen, George Zheng, Derek J. Fray, and Tom W. Farthing. "Direct electrochemical reduction of titanium dioxide to titanium in molten calcium chloride." nature 407.6802 (2000): 361-364.

11. Gordo, Elena, George Z. Chen, and Derek J. Fray. "Toward optimisation of electrolytic reduction of solid chromium oxide to chromium powder in molten chloride salts." Electrochimica Acta 49.13 (2004): 2195-2208.

12. Xiao, Wei, and Dihua Wang. "The electrochemical reduction processes of solid compounds in high temperature molten salts." Chemical Society Reviews 43.10 (2014): 3215-3228.

13. Inman, D., and S. H. White. "The production of refractory metals by the electrolysis of molten salts; design factors and limitations." Journal of applied electrochemistry 8.5 (1978): 375-390.

14. Li, S. X., M. F. Simpson, and S. D. Herrmann. “Oxygen Ion Oxidation Process on a Platinum Electrode in LiCl-Li2O at 650 C.” ECS Proceedings Volumes 2004.1 (2004): 171.

15. Jeong SM, Shin HS, Cho SH, Hur JM, Lee HS. Electrochemical behavior of a platinum anode for reduction of uranium oxide in a LiCl molten salt. Electrochim Acta. 2009;54(26):6335-6340. Doi:10.1016/j.electacta.2009.05.080

16. Chamberlain, Jarom, and F. Simpson Michael. "Corrosion of anode materials during direct electrolytic reduction of uranium oxide in molten LiCl-Li2O." Journal of Nuclear Materials 564 (2022): 153680.

17. Mullabaev, A. R., et al. "Anode processes on Pt and ceramic anodes in chloride and oxide-chloride melts." Nuclear Engineering and Technology 54.3 (2022): 965-974.

18. Kim, Sung-Wook, et al. “Electrochemical properties of noble metal anodes for electrolytic reduction of uranium oxide.” Journal of Radioanalytical and Nuclear Chemistry 311 (2017): 809-814.

19. Choi, Eun-Young, et al. “Electrolytic reduction runs of 0.6 kg scale-simulated oxide fuel in a Li2O-LiCl molten salt using metal anode shrouds.” Journal of Nuclear Materials 489 (2017): 1-8.

20. Wang, Dihua, and Wei Xiao. "Inert anode development for high-temperature molten salts." Molten Salts Chemistry. Elsevier, 2013. 171-186.

21. Yuan, Yating, et al. "Electrolysis of metal oxides in MgCl 2 based molten salts with an inert graphite anode." Faraday discussions 190 (2016): 85-96.

22. Park, Wooshin, et al. "Application of a boron doped diamond (BDD) electrode as an anode for the electrolytic reduction of UO2 in Li2O–LiCl–KCl molten salt." Journal of nuclear materials 432.1-3 (2013): 175-181.

23. Hur, Jin-Mok, Ju-Sun Cha, and Eun-Young Choi. “Can carbon be an anode for electrochemical reduction in a LiCl-Li2O molten salt?.” ECS Electrochemistry Letters 3.10 (2014): E5.

24. Vishnu, D. Sri Maha, et al. "Mechanism of direct electrochemical reduction of solid UO2 to uranium metal in CaCl2-48mol% NaCl melt." Journal of The Electrochemical Society 160.9 (2013): D394.

25. Motsegood, Perry N., James L. Willit, and Mark A. Williamson. "Development of Carbon Anodes for Use in Electrolytic Reduction of Uranium (IV) Oxide." Electrochemical Society Meeting Abstracts 230. No. 47. The Electrochemical Society, Inc., 2016.

26. Burak, Adam, Jarom Chamberlain, and M. F. Simpson. "Study of entrainment of Li2O in product from direct electrolytic reduction of UO2 in molten LiCl–Li2O. Part 1: Post-processing and analysis techniques." Journal of Nuclear Materials 529 (2020): 151913.

27. Gonzalez, Mario, et al. "Identification, measurement, and mitigation of key impurities in LiCl-Li2O used for direct electrolytic reduction of UO2." Journal of Nuclear Materials 510 (2018): 513-523.

28. Burak, A., J. Chamberlain, and M. F. Simpson. "Li2O entrainment during UO2 reduction in molten LiCl-Li2O: Part II. Effect of cathodic reduction mechanism." Journal of The Electrochemical Society 167.16 (2020): 166513.

29. Herrmann, S. D. Electrolytic Reduction of Spent Nuclear Oxide Fuel--Effects of Fuel Form and Cathode Containment Materials on Bench-Scale Operations. No. INL/CON-07-12182. Idaho National Lab.(INL), Idaho Falls, ID (United States), 2007.

30. Mos, Yvonne M., et al. “X-ray diffraction of iron containing samples: the importance of a suitable configuration.” Geomicrobiology journal 35.6 (2018): 511-517.

31. Singh, Balwant, et al. "Applications of synchrotron-based X-ray diffraction and X-ray absorption spectroscopy to the understanding of poorly crystalline and metal-substituted Iron oxides." Developments in Soil Science. Vol. 34. Elsevier, 2010. 199-254.

32. Sun, Xiao, et al. "Phase composition of iron oxide nanoparticles studied using hard X-ray absorption spectroscopy." The Journal of Physical Chemistry C 127.25 (2023): 12077-12083.